ELSEVIER

Nuclear Engineering and Design 189 (1999) 163–178

Nuclear Engineering and Design

Experimental simulation of microinteractions in large scale explosions

X. Chen, R. Luo, W.W. Yuen, T.G. Theofanous *

Department of Chemical and Nuclear Engineering, Center for Risk Studies and Safety, University of California, Santa Barbara, CA 93106, USA

Received 24 August 1998; accepted 24 December 1998

Abstract

The fragmentation behavior of molten steel drops forced to explode in sustained pressure fields is investigated. The effect of pressure amplitude, melt superheat, and coolant velocity is considered. The data include external images from high-speed movies, internal structures from simultaneously obtained flash X-ray radiographs, and solidified debris size distributions and morphology from scanning electron micrographs. The results demonstrate the importance of all three parameters studied on both the rates and extent of the interaction/fragmentation.

1. Introduction

The purpose of this paper is to extend previous work on the microinteractions of steam explosions (Yuen et al., 1994; Chen et al., 1997) towards reactor materials and realistic conditions. Specifically, we take up steel at temperatures up to 1650°C (200°C superheat), and shock pressures approaching those of large scale explosions at hundreds of atmospheres and well into the thermodynamic supercritical region. As in our previous work, we make use of the SIGMA facility, modified for the present purposes with a new melt generation and delivery system capable of reaching 2000°C; hence the SIGMA-2000 name in this version.

The concept of these experiments derives from the recognition that the key mechanisms that support the propagation of multiphase thermal detonations are dominated by the high pressures of the detonation wave itself (hundreds of atmospheres), rather than the phase-change-induced

* Corresponding author. Tel.: +1-805-8934900; fax: +1-805-8934927.

E-mail address: theo@theo.ucsb.edu (T.G. Theofanous)

0029-5493/99/$ - see front matter
PII: S0029-5493(99)00032-1

high velocities found at the low ambient (atmospheric) pressures of previous work. Thus, inducing a sustained shock of an appropriate amplitude allows us to simulate a large scale detonation with a single melt drop. This in turn allows detailed observations of the kind impossible in actual large scale detonations. The arrangement is that of a hydrodynamic shock tube —the SIGMA facility. By introducing voids (gas bubbles) we can further represent a two-phase coolant, especially in regards to the much higher (compared to single phase liquid) coolant velocities attained behind the shock.

The microinteractions concept refers to the highly localized contact of the fragmenting debris with the surrounding coolant. It gives rise to the creation of a debris-rich zone (the m-fluid), which provides the rapid feedback that sustains the propagation. The coolant that surrounds this zone participates only as a compressible medium (does not interact thermally), and it is gradually entrained to mix with continually produced debris (fine fragments coming off the parent drop), both then added to the m-fluid. Previous models/codes based on the uniform mixing of Board and Hall have failed to produce an adequate feedback (unrealistically high fuel concentrations and fragmentation rates were required), and it is clear now that microinteractions constitute a first order effect. If as a first approximation the m-fluid is considered to be in local thermodynamic equilibrium, the constitutive law for microinteractions needs only the coolant entrainment and debris creation (fragmentation) rates. Still, as a first approximation, in ESPROSE.m these two quantities are made proportional to each other with an entrainment coefficient, f_e, to be determined experimentally, vz

$$E = f_e F_r \frac{\rho_c}{\rho_f} \tag{1}$$

where ρ_c and ρ_f are the density of the surrounding coolant and fuel, respectively. The problem is completely specified if we further supply F_r, the fragmentation rate and in ESPROSE.m, this is done in terms of a hydrodynamic fragmentation formulation (Chen et al., 1997) which yields

$$F_r = \frac{\theta_f \rho_f \gamma_t}{t_f} \tag{2}$$

where θ_f *is* the local volume fraction of the fuel, t_f *is* a 'breakup' time which can be estimated based on instantaneous Bond number formulation (Yuen et al., 1994) and γ_t represents a thermal augmentation factor. Previous work with molten tin drops in SIGMA (Chen et al., 1997) suggested that while γ_t may be as large as 4 at 'low' pressures (1000 psi) it approaches unity at high, supercritical pressures. With steel melts we have twice the heat capacity, and four times the latent heat of tin, thus we can expect at even stronger thermally-driven fragmentation, albeit it should also diminish at high pressures, leading to a $\gamma_t \to 1$ at a sufficiently high level.

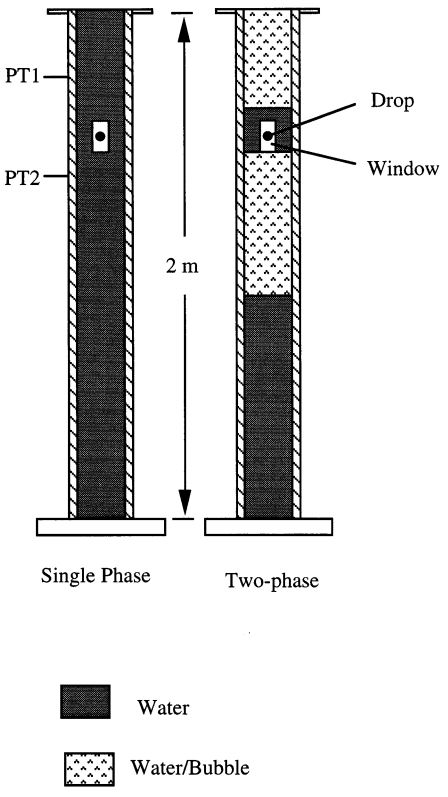

Fig. 1. Schematic of the void fraction distribution for the single-phase and two-phase runs (the figure is in scale in the vertical direction only).

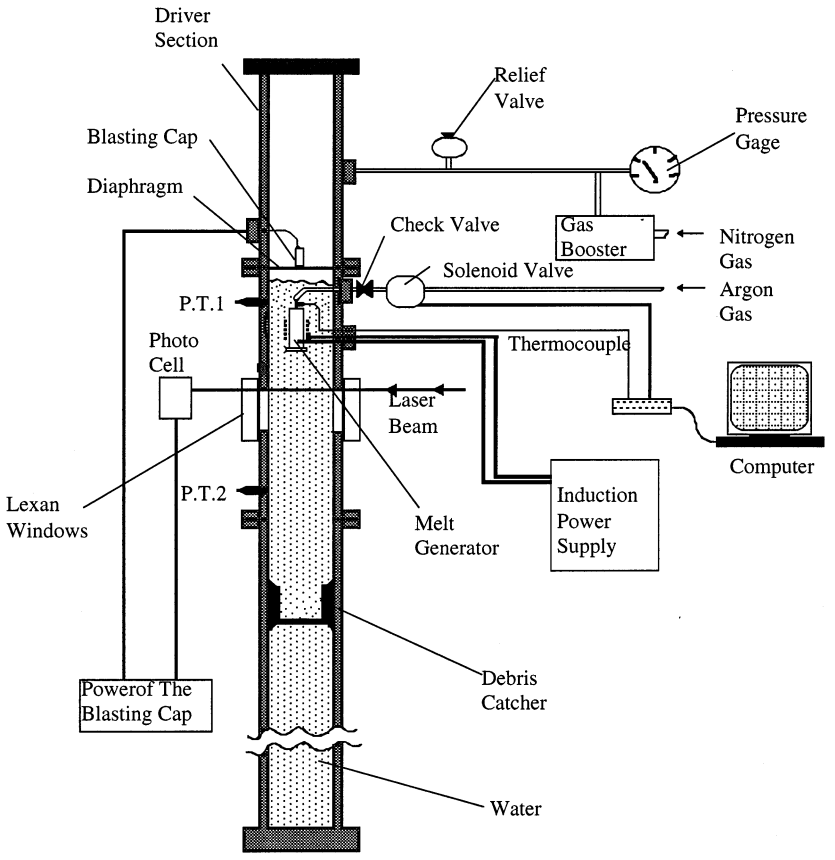

Fig. 2. Schematic of SIGMA-2000 facility (not to scale).

Table 1
Test conditions of the six runs

Run ID	P (bar)/T (°C)	Void fraction	Bo	X-ray time (ms)
S-1-16.2	68/1620	0	34	–
S-4-15.5	265/1550	0	300	0.32
S-4-16.5a	265/1650	0	300	–
S-4-16.5b	265/1650	0	300	–
S-4-15.5 (0.06)	265/1550	0.06	1500	0.12
S-4-16.5 (0.06)	265/1650	0.06	1500	0.22

Clearly, to check these ideas and to provide the basis for further refinements, we need quantitative access to the m-fluid; that is, its detailed structure and composition, as well as their evolution with time, in the tens of ms scale. For this purpose, we use high speed movies, and a simultaneous flash X-ray shot at a selected instant in time. The radiography, made quantitative, can reveal the amount of debris and its spatial distribution. The corresponding visual image (from the movie) shows the external appearance of the composite volume, made up by the m-fluid and the parent

drop. They together can go a long way towards the purpose noted above. The optimization of these data is significantly restricted, however, by the sustained high pressure required for the simulations; that is, restricted visual access and burdened optical path (thick lexan windows).

The confinement, on the other hand, allows us to catch the resulting debris, and the simulation affected in the experiments makes it possible, for the first time, to take a glimpse into what is produced in large scale explosions. As we will see, size distributions and the morphologies revealed in scanning electron micrographs, as functions of the experimental variables, are quite complementary to the explosion visualization data, and suggestive of their own.

2. The experiment

The SIGMA facility has been described previously (Chen et al., 1997) and only a brief summary is needed here. The main component is the 'expansion section,' a 2 m long tube, with square,

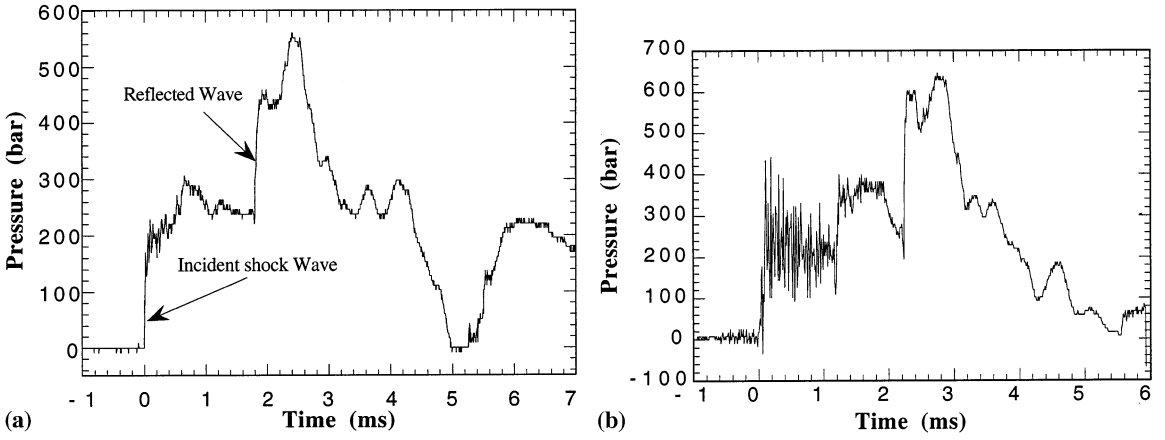

Fig. 3. Pressure transient as recorded by PT-2 in runs S-4-16.5a and S-4-16.5 (0.06).

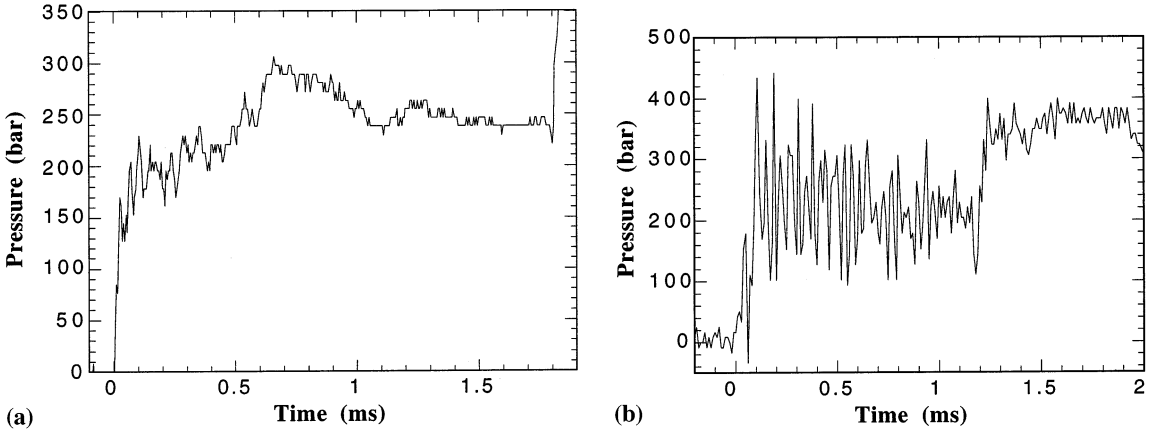

Fig. 4. Pressure transients of Fig. 3, on an expanded time scale.

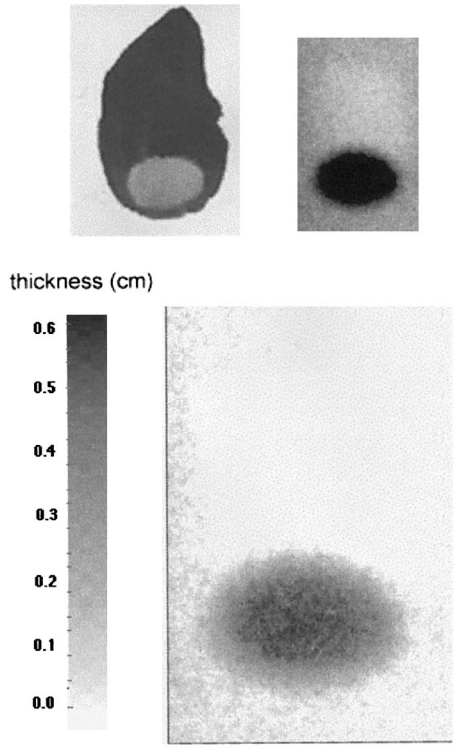

Fig. 5. The visible image, X-ray image and mass distributiion contours of a molten steel drop (1650°C) in 20°C water in free-fall (prior to shock arrival).

5×5 cm, cross section, as shown in Fig. 1. In the single phase mode the tube is filled up with water, while with two phases the tube was operated with imbedded gas bubbles, as illustrated in Fig. 1. A stationary, well-characterized configuration of known void fraction (6%) was obtained by uniformly distributing air trapped in thin plastic sheets, such as used in packing. The characteristic dimension in the experiments was ~ 1 cm. In these experiments the initial pressure of the expansion section was always ~ 1 atmosphere. In Fig. 1, we can also see the window and the melt drop in it. Positions PT1 and PT2 show the locations of pressure measurement.

The pressure wave was generated by releasing the pressure (rupturing a pre-scored steel diaphragm) from the driver section, shown with a diagrammatic of the whole facility in Fig. 2. In this figure, we can also see the charging/venting system, the timing and control circuitry, and the melt generating device. This device is specially designed to miniature scale so it can be accommodated inside the tube and present little disturbance to the pressure wave. It can reproducibly release a single, 1 g, drop of steel melt, at any desired temperature up to 2000°C. The drop is released 6 cm above the upper edge of the window, and the intent is to hit it at this position so it can be observed as it fragments, translating downwards. Clearly the synchronization requirements for this experiment are extremely challenging.

Movies were obtained with a drum camera at 50 000 frames per second, through a mirror, so as to allow the positioning of the X-ray tube and the cassette film holder along the optical path of the windows. Light for the movie was admitted through a smaller side window (not shown). The radiography contained 'witness' pieces, which with highly reproducible film exposure, development, and reading procedures allowed consistent calibration and quantification of the debris distribution (projected optical thickness). Integration of these distributions reproduced the whole mass of drop to within $\pm 10\%$, which is indicative of the accuracy of the measurement. The images from the high speed movies were digitized and converted to volumes (of the interaction zone) assuming cylindrical symmetry.

The debris was caught using the device illustrated in Fig. 2 as the 'catcher.' It was made of hard plastic to a snug fit, occupying the whole tube cross section, but free to slide up and down under the incident and reflected pressure waves. The mass recovery was good down to some tens of micron scales, where the mass lost appeared to increase with the intensity of the explosion. This extremely fine fraction is called 'non-recovered' and is reported lumped together with the 'fines' ($0 < d < 100$ μm).

3. Experimental results

The present experimental program involved six tests, all with steel material, at conditions summarized in Table 1. We covered two pressure levels,

1000 psi (68 bar) and 4000 psi (265 bar), three melt temperatures, corresponding to superheats of 100, 170, and 200°C, and two coolant media, single-phase liquid, and 6% void, bubbly two-phase mixture. As seen in the table, the same driving pressure creates significantly higher velocities (Bond numbers) in the two-phase medium. In all tests the liquid (water) temperature was as 20°C. In the identifying code for each run, the first digit refers to the shock pressure level (in kpsi), the second number refers to the droplet temperature (in hundreds of °C), and the last number in parenthesis, if present, indicates a two-phase medium and the void fraction in it.

The overall wave forms obtained (location PT2) in the single and two-phase media are shown in Fig. 3a and b respectively. The detailed pressure transients in the time scales of the explosion phe-

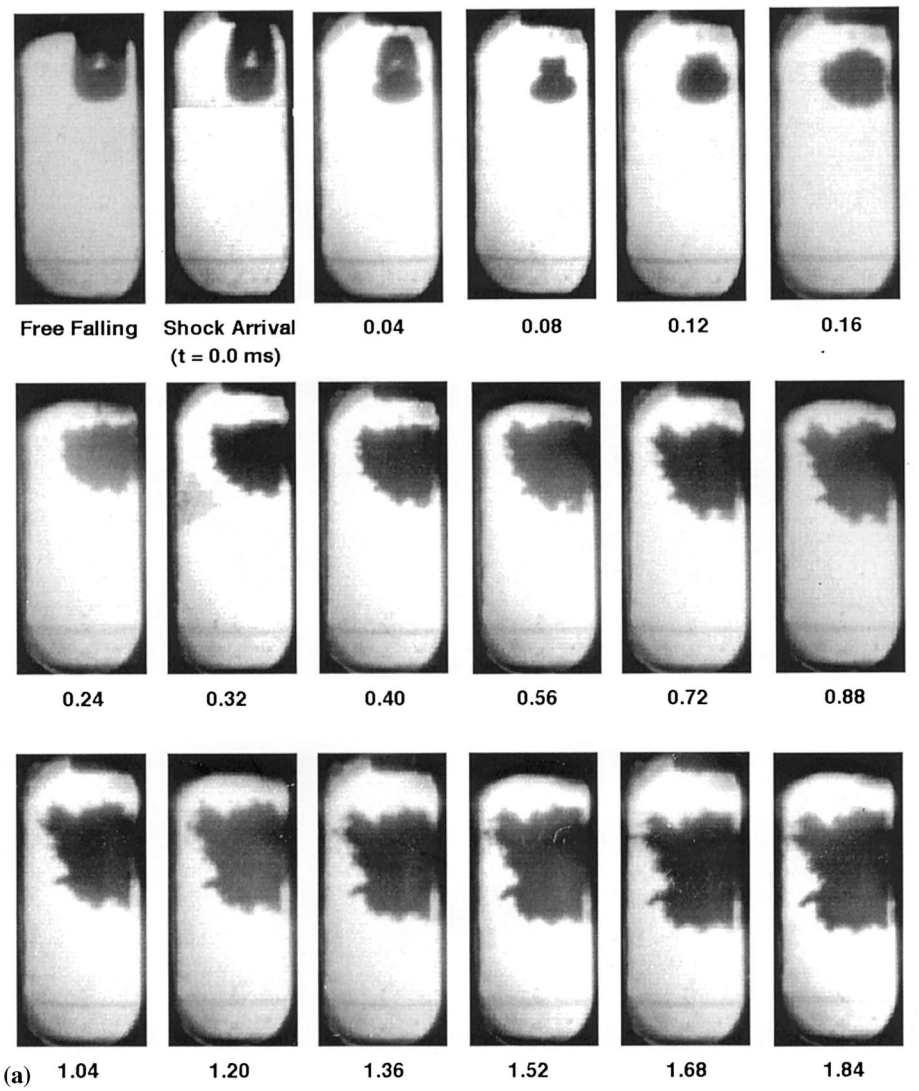

Fig. 6a. High speed movie images of run S-1-16.2.

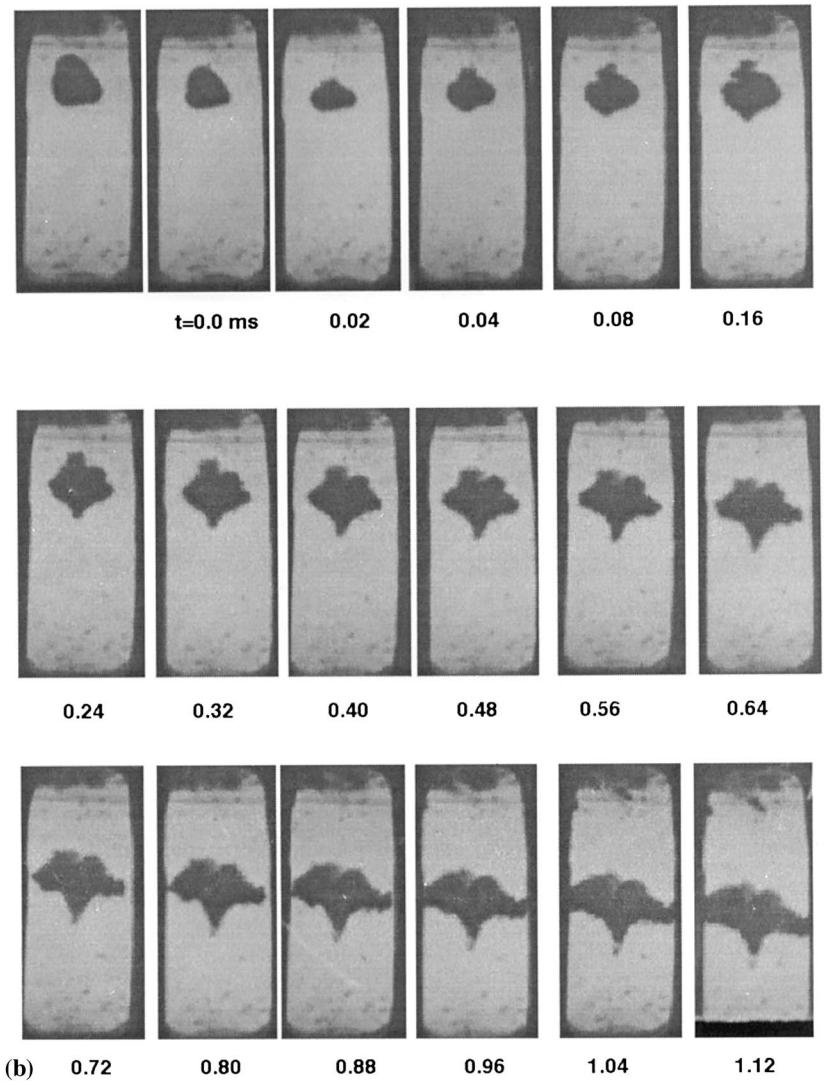

Fig. 6b. Run S-4-15.5.

nomenon can be seen in the expanded scales of Fig. 4a and b respectively. Remarkable in and 3b and 4b is the high frequency oscillation in the primary (incident) wave. These are created by the compression and rarefaction events that follow collapse of individual gas bubbles, i.e. mini-water-hammers and mini-venting events as these waves advance ahead into uncompressed regions, respectively. Also interesting is the reflection at 1.3 ms in Fig. 3b. It derives from the lower two-phase/liquid interface (see Fig. 1); at this point all voids have been compressed, and all subsequent signal is typical of a single-phase medium. Peak amplitudes in the two-phase signal reach almost twice the driving pressure. As we have seen elsewhere (Theofanous and Yuen, 1998; Theofanous et al., 1999) these pressures are quantitatively predictable in all their detail. In the expanded scale

figures we note that the rise time in the single phase run is only a small fraction of 100 μs, while in the two-phase condition it may be as long as ~100 μs.

Video and X-ray images of a steel drop in a free-fall condition are shown in Fig. 5, together with the quantitative, reconstructed image of the radiograph. We can see a rather pronounced vapor bubble, much larger than expected at such highly subcooled film boiling, and this is typical of all runs, with the exception that it is considerably smaller at the lower melt temperatures (100 vs 200°C superheat). We have not analyzed this aspect yet in detail, but it appears that the bubble is considerably stabilized by the hydrogen produced in the metal–water reaction; that is, the non-condensible interfering with condensation. The images in Fig. 5 constitute a 'standard' (the initial condition), against which the images obtained during the interaction are to be compared in studying the behavior.

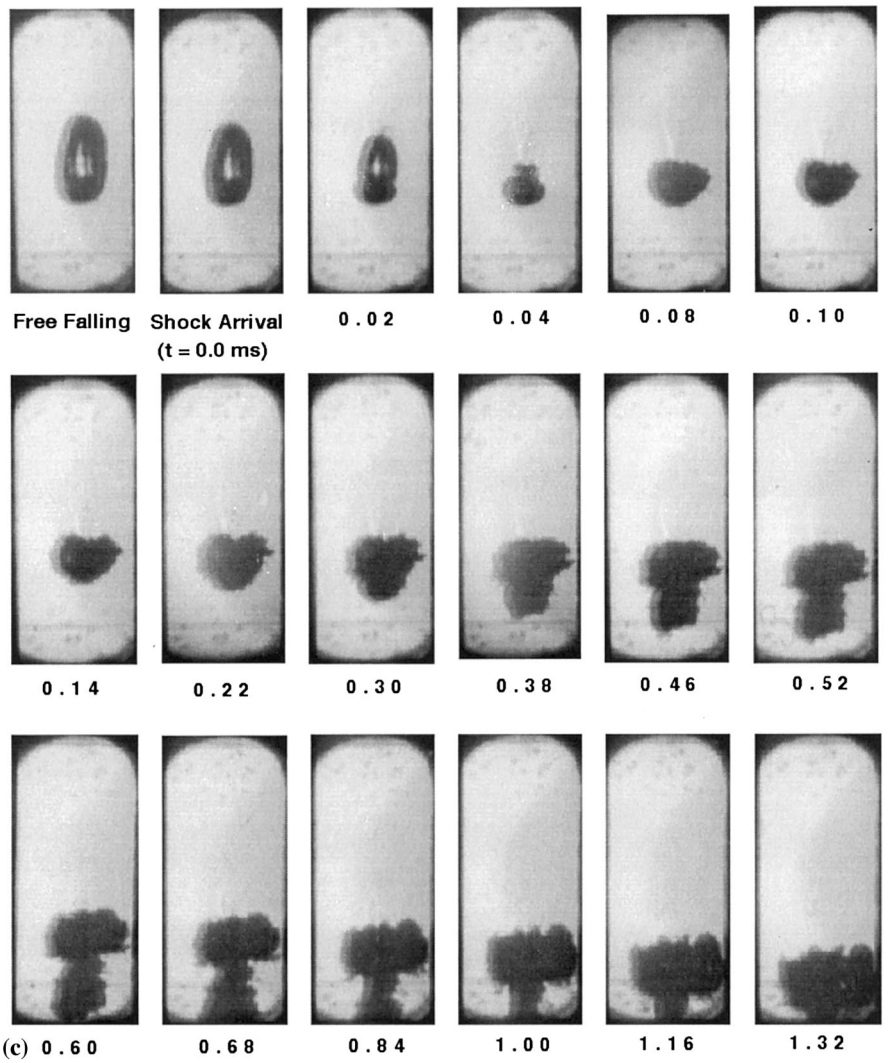

Fig. 6c. Run S-4-16.5a.

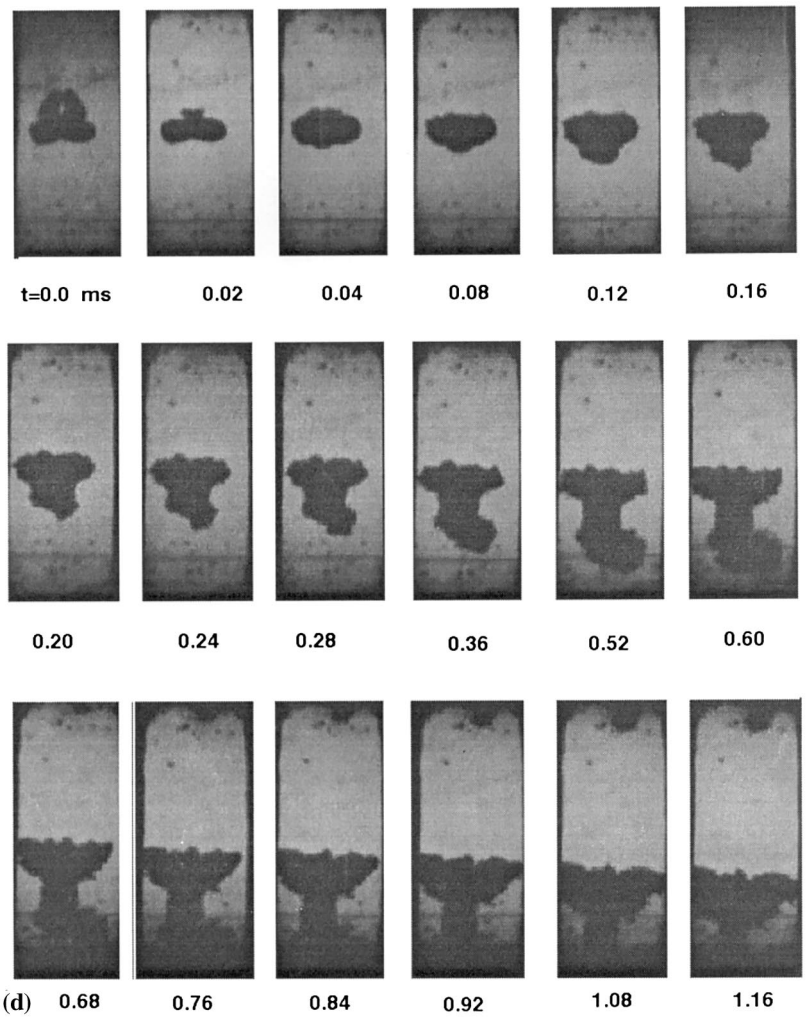

Fig. 6d. Run S-4-16.5b.

In the window area the free-fall speed was 0.7 m/s, while coolant velocities behind the 1000 and 4000 psi waves were 4.5 and 15 ms, respectively. In the two-phase runs the coolant velocity reached 38 m/s. The corresponding Bond numbers are shown in Table 1.

The high-speed movie images for all six runs are shown in Figs. 6a, 6b, 6c, 6d, 6e and 6f. We can immediately observe that the 'explosions' occur in the time frame of 100 μs, and that the apparent intensity is reduced in the lower superheat runs. Also, we can discern the confining effect of the higher shock pressures on the microinteractions; that is, the growth of the mixing zone (m-fluid) surrounding the parent drop. At a more detailed level, we note that in the 'low' pressure run (6a) the growth of the m-fluid is continuous, and proceeds rather symmetrically but with highly structured front. By contrast, such a relatively symmetric growth period is rather limited in the corresponding (same temperature) high pressure runs (6c, 6d), it being followed by

discrete events localized at the rear face of the drop; there is a single such event in one of these runs (6d) and two sequential and superposed such events in the other (6c). The lower superheat run corresponding to these (6b) exhibits a faint attempt for such a local event, but it remains rather undeveloped. Finally, the two-phase condition (high coolant velocities) seems to promote the interaction sufficiently to overcome the confining effect of pressure, but the structure of the expanding fronts is completely different with only the large scales remaining (compare 6f to 6a).

The available X-ray images are shown in Figs. 7a, 7b and 7c. Comparison with Fig. 5 shows significant fragmentation and mixing, even in the time frame of 100 μs. Comparisons among themselves indicate the augmenting effect of velocity and superheat (7c against 7a), and the importance of the interactions within the shock front (pressure rise transient region) as seen on 7b. Remarkable also are the downward-facing concave shapes of the main debris mass at lower superheat runs

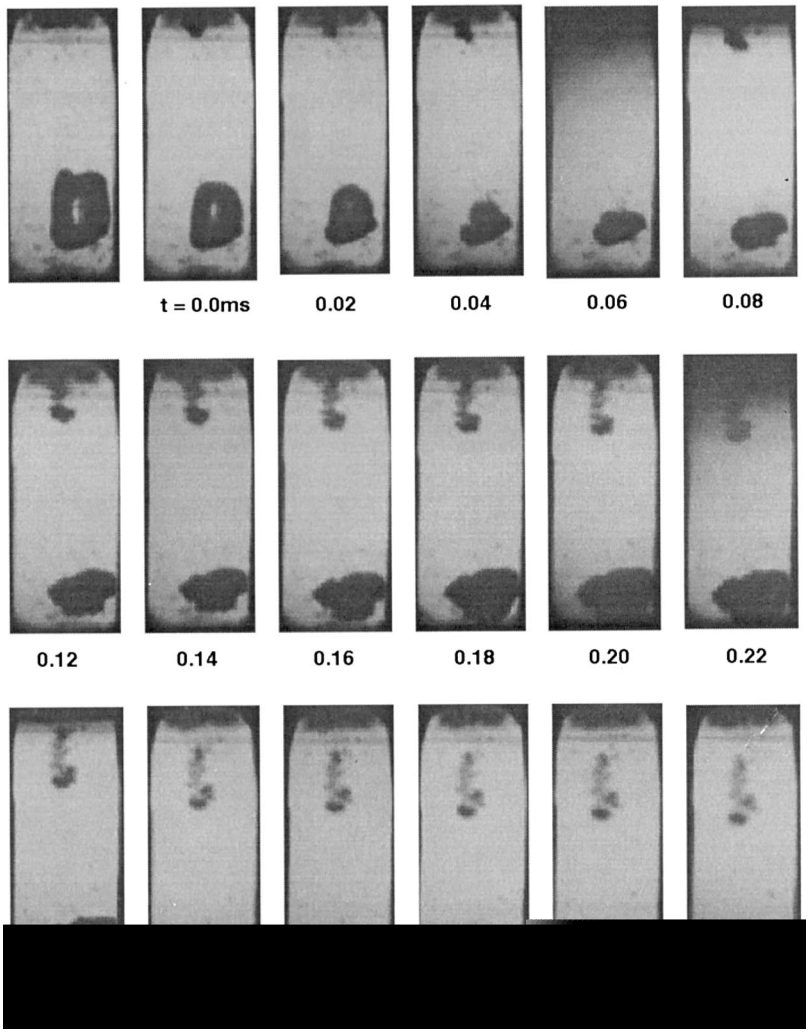

Fig. 6e. Run S-4-15.5 (0.06).

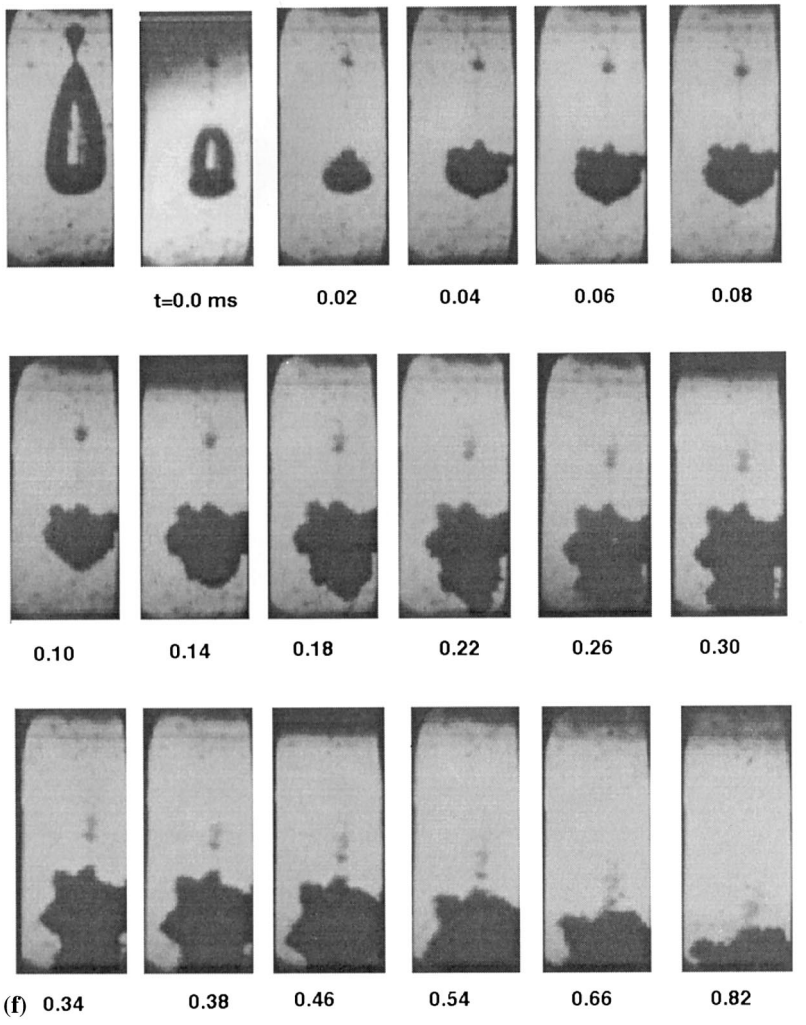

Fig. 6f. Run S-4-16.5 (0.06).

(7a and 7b), as distinct from the convex shape seen in the higher superheat (7c). The latter shows the characteristic 'strands' of 'swept' debris observed in our previous hydrodynamic fragmentation experiments using mercury drops (Theofanous et al., 1979).

The debris size distributions are shown in Fig. 8. Some very fine debris could not be recovered, even with the extreme care in procedure employed. For the single phase runs, this was limited to only $\sim 5\%$ or less of the total mass, but for the more extensively fragmented two-phase runs these amounts could reach $\sim 20\%$. These are included in the 0–0.1 μm sieve fraction reported in Fig. 8. Some very interesting contrasts and trends can now be seen in this figure. First is the contrast due to pressure in the single phase runs. At 'low' pressure all mass was fragmented to submillimetre fragments, and about half of it was below 300 μm. At high pressure, on the other hand, most of the mass remained in relatively large, but porous particles. The effect of temperature on these two runs

seems rather negligible. Second is the contrast due to the presence of two-phase coolant. As we have seen this causes much higher coolant velocities (for the same driving pressure), and a highly 'structured' pressure front. In Fig. 8, we see that the result is much greater yield (than the single phase run) of fines, although some non-negligible fraction remained above the 1 mm scale. In these two runs we also see a rather pronounced effect of superheat on the fines yield.

Representative scanning electron micrographs (SEM) of the debris are shown in Figs. 9a, 9b, 9c and 9d. In these, remarkable is the fine scale structures on the particles themselves. Allowing the first actual view of material that has participated in a large-scale steam explosion, these photographs are suggestive of mechanisms (as a multi-interactive, sequenced process) and constitute probably one of the most important results of this investigation.

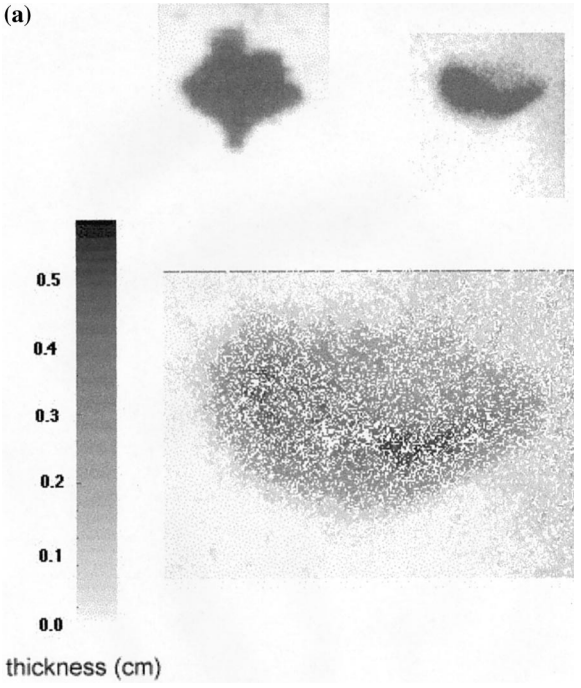

Fig. 7a. Visible image, X-ray image and the mass fraction contours for a fragmenting drop at 0.32 ms after shock arrival for run S-4-15.5. The top two images are on the same scale.

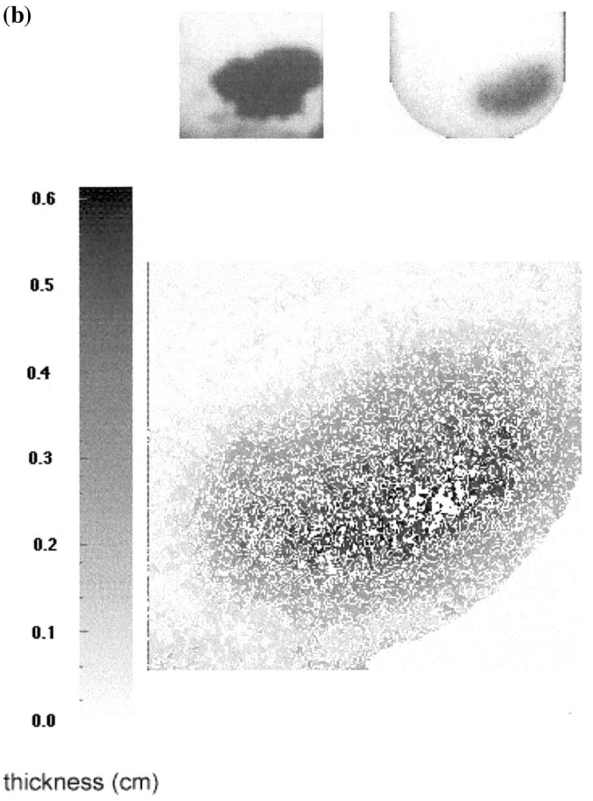

Fig. 7b. At 0.12 ms after shock arrival for run S-4-15.5(0.06).

In Fig. 10, we show how a characteristic length scale of the microinteractions zone evolves with time as deduced from the high-speed movies for all six runs. The data for this figure were obtained by digitizing the external zone images and converting these to volume, V, by assuming cylindrical symmetry. The excess volume then, V-V_0, where V_0 is the initial droplet volume, is normalized by the initial surface area of the drop, the result representing a rough indication of the 'thickness' of the microinteractions zone. It is interesting in Fig. 10 to note the reproducibility of the two repeat runs. Also interesting is the confirmation of above-noted trends (from the debris

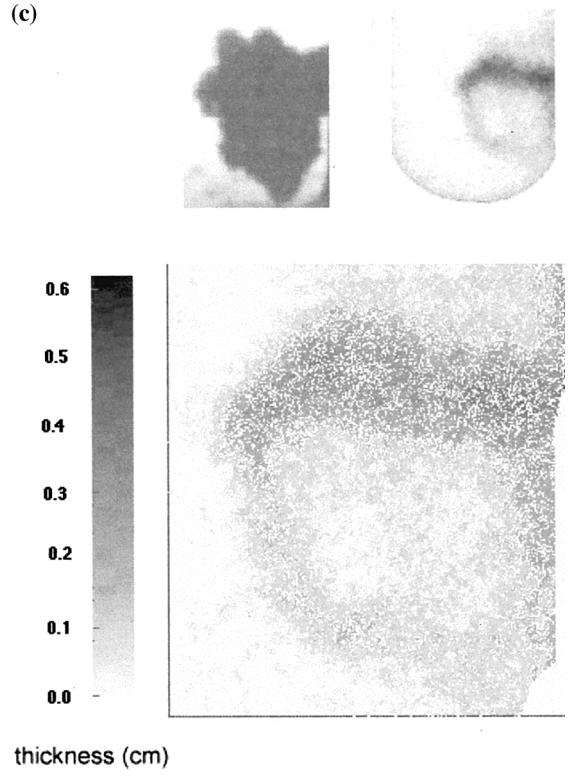

Fig. 7c. At 0.22 ms after shock arrival for run S-4-16.5(0.06).

analysis); namely, the augmenting effect of melt superheat, of the 'low' pressure, and of the high coolant velocity (two-phase runs). Of special interest is the high-superheat, two-phase run, and it suggests the need to further focus on the details of the shock front, under such two-phase conditions, and to further resolve the microinteractions behavior at still higher pressures.

4. Conclusions

The experimental data presented in this paper bring us an important step forward in our quest for the microinteractions that sustain propagating large-scale explosions with reactor materials. A key, and unique feature of this data is the sustained high pressure field imposed, so as to simulate the 'reaction zone' environment in actual explosions. The present steel data are complementary to previous ones obtained with tin, mercury, and gallium. Important differences are noted, and they appear connected to the much greater (one order) heat content of the steel drops. Also, we find significant augmentation of the interactions

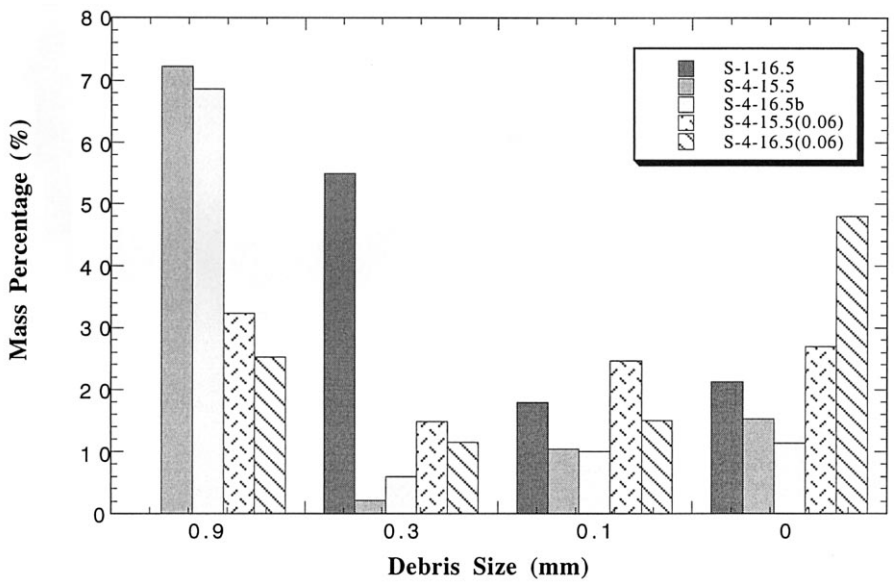

Fig. 8. Debris size distribution expressed by the retaining sieve size. The amounts shown at zero size include the non-recovered debris (see text).

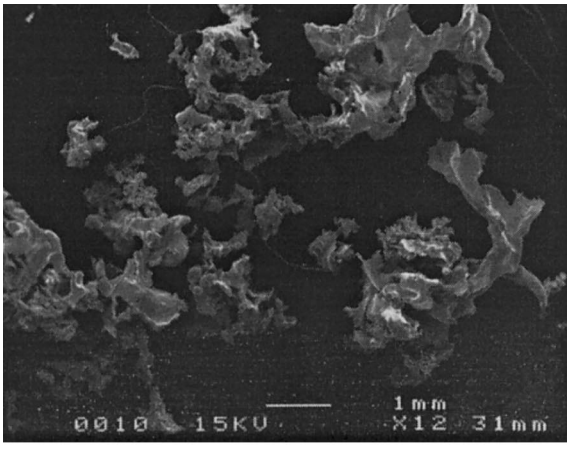

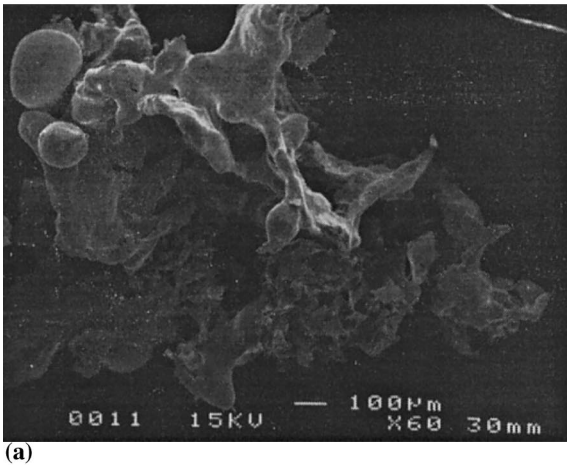

(a)

Fig. 9a. SEM photographs for run S-4-15.5. The top photograph is for a 'large' particle and the bottom photograph is for a 'small' particle.

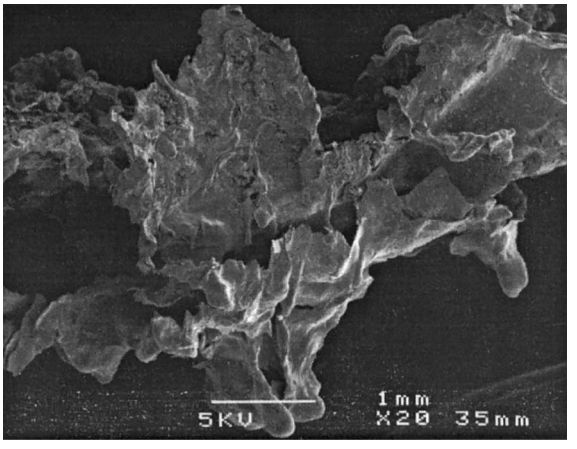

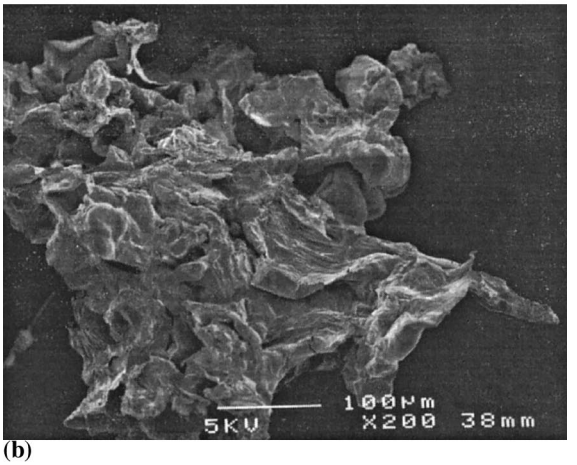

(b)

Fig. 9b. Run S-4-16.5a.

with melt superheat and coolant velocity. High pressures appear to have a dampening effect, although even higher pressures than those employed here would appear to be needed to get into a hydrodynamics-dominated regime. The interactions proceed on the time scale of tens to hundreds of μs, and this brings out the importance of the wave front, especially as it propagates through media with a highly compressible (vapor) phase. The data presented herein can be used in testing concepts and models for microinteractions, and the trends observed provide a basis for refocusing the experimental conditions toward better simulation of large-scale detonations in SIGMA, and finer resolution of the measurements.

Acknowledgements

This work was supported under the ROAAM program carried out for the US DOE's Advanced Reactor Severe Accident Program (ARSAP), under ANL subcontract No. 23572401 to UCSB.

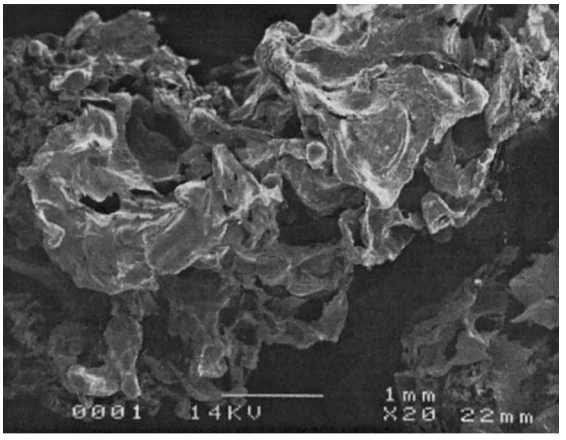

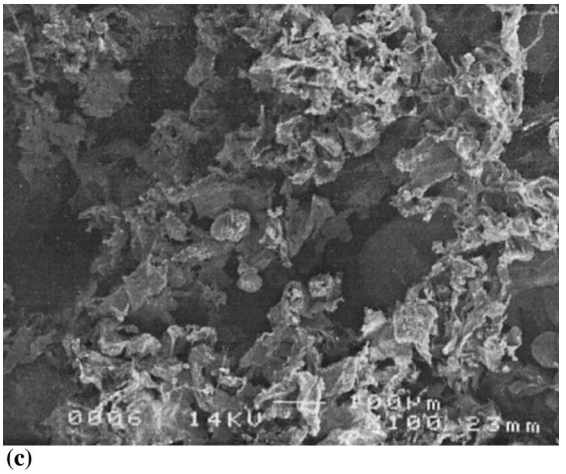

(c)

Fig. 9c. Run S-4-16.5 (0.06).

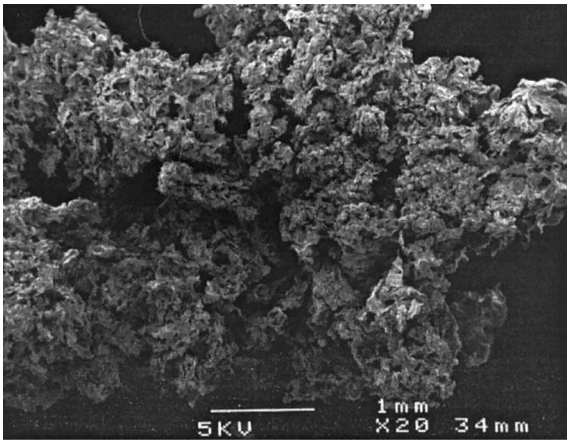

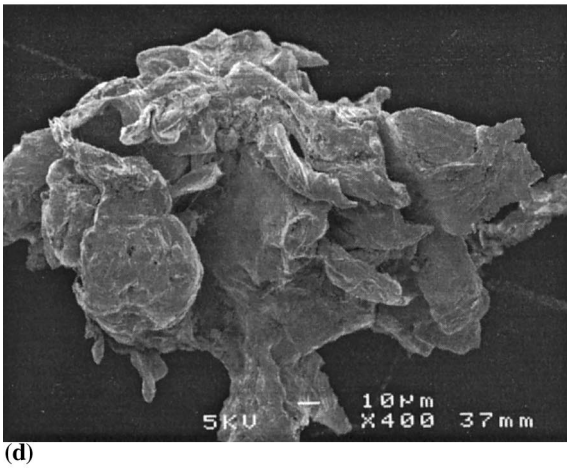

(d)

Fig. 9d. Run S-1-16.2.

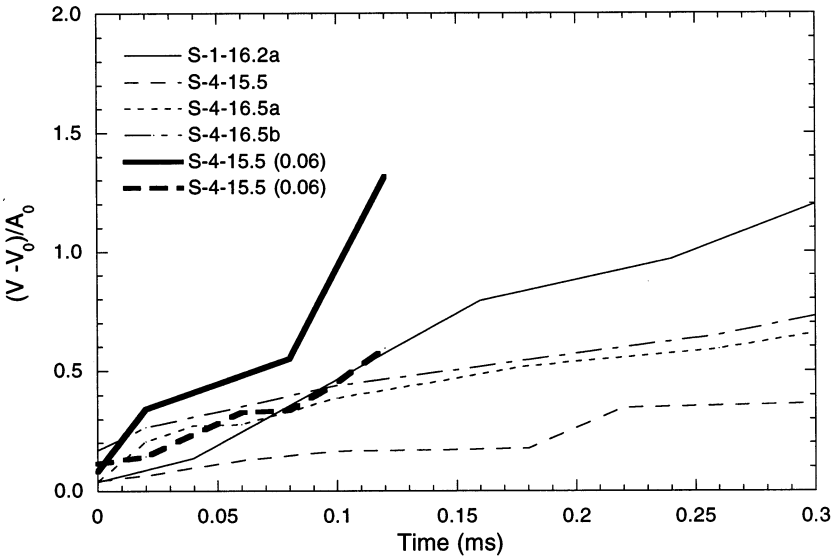

Fig. 10. Growth of the 'thickness' of the microinteractions zone for the six runs. (Time 0 corresponds to the time of the initial bubble collapse around the drop.)

References

Chen, X., Yuen, W.W., Theofanous, T.G., 1997. On the constitutive description of the microinteractions concept in steam explosions. Nucl. Eng. Des. 177, 303–319.

Theofanous, T.G., Yuen, W.W., Freeman, K., Chen, X., 1999. The Verification Basis of the ESPROSE.m Code. Nucl. Eng. Des., in press.

Theofanous, T.G., Saito, M., Efthimiadis, T., 1979. Fuel-coolant interactions and hydrodynamic fragmentation, Proceedings of the International Meeting on Fast Reactor Safety Technology, Vol. III, Seattle, WA, 19–23 August, pp. 1568–1577.

Theofanous, T.G., Yuen, W.W., 1998. Fundamentals of boiling and multiphase flow under extreme conditions, heat transfer, Proceedings of the 11th IHTC, Vol. 1, Kyongju, Korea, 23–28 August, pp. 131–147.

Yuen, W.W., Chen, X., Theofanous, T.G., 1994. On the fundamental microinteractions that support the propagation of steam explosions. Nucl. Eng. Des. 146, 133–146.